

## Nanoscale Control of Surface Immobilized BMP-2: Toward a Quantitative Assessment of BMP-Mediated Signaling Events

Elisabeth H. Schwab,<sup>†,‡</sup> Theresa L. M. Pohl,<sup>†,‡</sup> Tamás Haraszti,<sup>†,‡</sup> Gerburg K. Schwaerzer,<sup>§</sup> Christian Hiepen,<sup>§,||</sup> Joachim P. Spatz,<sup>†,‡</sup> Petra Knaus,<sup>§,||</sup> and Elisabetta A. Cavalcanti-Adam\*,<sup>†,‡</sup>

<sup>†</sup>Department of Biophysical Chemistry, Institute of Physical Chemistry, University of Heidelberg, INF 253, 69120 Heidelberg, Germany

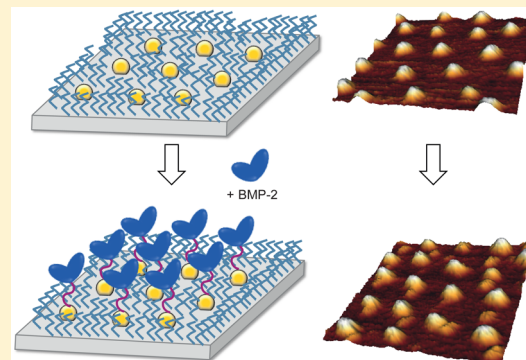
<sup>‡</sup>Department of New Materials and Biosystems, Max Planck Institute for Intelligent Systems, Heisenbergstr. 3, 70569 Stuttgart, Germany

<sup>§</sup>Institute for Chemistry and Biochemistry, Freie Universität Berlin, Thielallee 63, 14195 Berlin, Germany

<sup>||</sup>Berlin-Brandenburg School for Regenerative Therapies (BSRT), Charité Campus Virchow-Klinikum, Augustenburger Platz 1, 13353 Berlin, Germany

### S Supporting Information

**ABSTRACT:** In this work we determine the impact of surface density of immobilized BMP-2 on intracellular signal transduction. We use block copolymer micellar nanolithography to fabricate substrates with precisely spaced and tunable gold nanoparticle arrays carrying single BMP-2 molecules. We found that the immobilized growth factor triggers prolonged and elevated Smad signaling pathway activation compared to the same amount of soluble protein. This approach is suitable for achieving controlled and sustained local delivery of BMP-2 and other growth factors.



**KEYWORDS:** BCMN, gold nanostructures, BMP-2, covalent immobilization, cell signaling

Bone morphogenetic proteins (BMPs) belong to the transforming growth factor- $\beta$  (TGF- $\beta$ ) superfamily and exert important functions. During embryonic development and until adulthood they regulate a plethora of cellular processes such as proliferation, differentiation, cell motility, and survival, depending on the cellular context.<sup>1–3</sup> In particular, BMP-2 promotes the differentiation and maturation of osteoblasts and converts the differentiation of myoblasts into osteoblasts.<sup>4</sup> Because of its ability to induce de novo bone formation in vivo, BMP-2 has been used in spine surgery and tissue engineering approaches.<sup>5–7</sup> However, BMP-2 has pleiotropic functions; it is involved in maintaining the homeostasis of several organs, whereas abnormal BMP signaling leads to the manifestation of different human diseases including bone and vascular disorders and cancer.<sup>8,9</sup> Thus, several concerns have recently arisen because of the high amount of protein used in these procedures. Uncontrolled release of the protein from the site of application and uncontrolled effects at distant sites represent further challenges for clinical applications.

In living systems, BMPs exist in soluble as well as in matrix-bound forms.<sup>10</sup> Several studies have shown that tethered molecules regulate cell behavior quite distinctly from their freely diffusible form in the *in vivo* environment.<sup>11</sup> A variety of delivery systems for the presentation of tethered growth factors

onto substrates, such as noncovalent (e.g., entrapment or ion complexation) and covalent immobilization strategies, have been developed.<sup>12</sup> The major advantage of growth factor immobilization is improved efficiency, i.e., a small amount, and controlled presentation of the molecule. However, approaches based on protein modification (introducing artificial domains or peptide tags) have been shown to lead to unpredictable outcomes since these modifications affect cell behavior or hinder the biological activity of the growth factor.<sup>13</sup> Alternatively, to achieve protein immobilization, the substrate can be first decorated with a bifunctional molecule, which is linked to specific groups or residues of the protein.<sup>14–16</sup>

We previously reported the covalent immobilization of recombinant human BMP-2 homodimers onto surfaces by using a self-assembled monolayer consisting of an heterobifunctional linker, 11-mercaptopoundecanoyl N-hydroxysuccinimide ester (MU-NHS), thereby retaining both the protein's short- and long-term biological activity.<sup>15,16</sup> Here we present an approach, based on the same protein immobilization strategy, to selectively bind BMP-2 to gold nanoparticles arranged on the

**Received:** September 29, 2014

**Published:** February 10, 2015

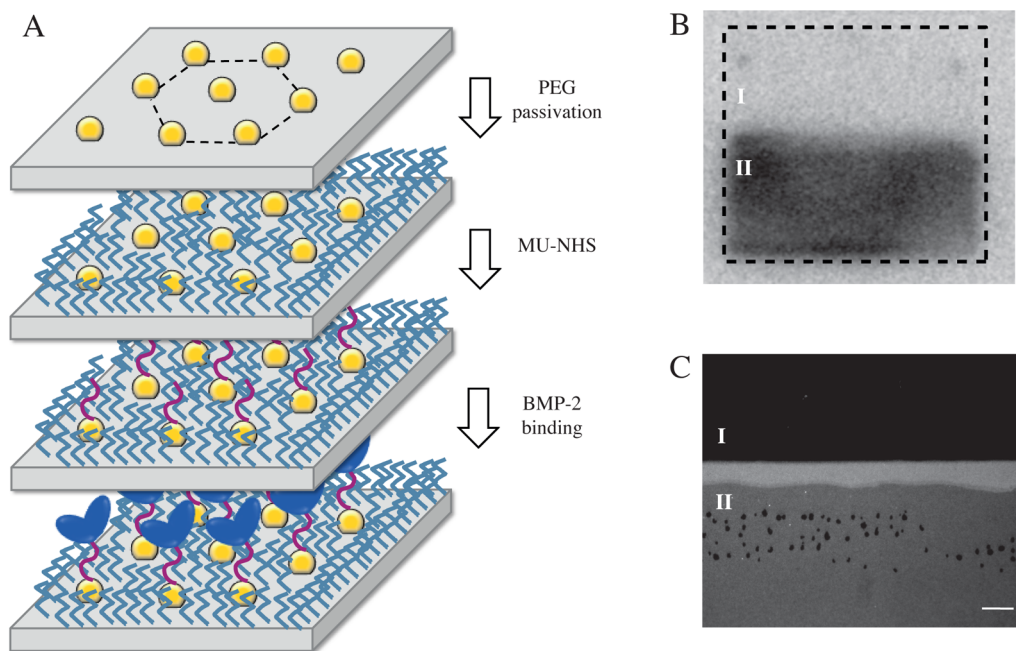


**Figure 1.** Preparation and detection of surface immobilized BMP-2. (A) Fabrication of nanostructured surfaces presenting BMP-2 covalently bound to gold nanoparticles. Gold nanoparticle arrays are produced by block copolymer micellar nanolithography. The space between the nanoparticles is covered with a layer of polyethylene glycol (PEG) to prevent unspecific adhesion of proteins and cells. Subsequently, the surfaces are incubated with a heterobifunctional linker (MU-NHS) that selectively binds to gold. Next, BMP-2 is immobilized on the functionalized gold nanoparticles via covalent binding of its primary amines to the linker. (B) Phosphorimaging of radiolabeled BMP-2. The protein is covalently immobilized on gold nanoparticles, which decorate only the lower part of a coverslip (darker area indicated with II), whereas the upper part is only coated with the PEG layer (brighter area indicated with I). (C) A representative fluorescence micrograph of part of a nanostructured coverslip presenting BMP-2 covalently bound to gold nanoparticles. Indirect immunofluorescence labeling of the protein, immobilized on the surface as in panel B, results in a fluorescence signal from the part of the substrate where BMP-2 is covalently bound to the gold nanoparticles (bottom part of the image, II) and not from the protein repellent side of the substrate (upper part of the image, I). The scale bar in panel C is 20  $\mu$ m, whereas the image in panel B shows the entire substrate (20 mm  $\times$  20 mm).

surface in hexagonal arrays. The spacing and the size of the gold nanoparticles are precisely tuned, thus offering the unique advantage of controlling the amount of immobilized protein at molecular level. In fact, since each particle is small enough to serve as anchor point for a single immobilized BMP-2 homodimer (iBMP-2), the local amount of the protein depends on the number of nanoparticles. By varying the distance between the BMP-2 functionalized gold nanoparticles, we determine the impact of ligand surface density on BMP-dependent intracellular signal transduction. Thus, with this unique setup we are able to assess, at unprecedented level, the minimum concentration (ranging from <0.5 to >3 ng/cm<sup>2</sup>) of surface-bound growth factor for initiating individual signal pathways.

Gold nanoparticle arrays were fabricated using block copolymer micellar nanolithography (BCMN) as previously reported.<sup>17,18</sup> Unspecific protein adhesion was prevented by depositing a layer of polyethylene glycol (PEG silane MW 2000) on the glass surface between the gold nanoparticles.<sup>19</sup> BMP-2 was then selectively immobilized on the nanoparticles via the MU-NHS heterobifunctional linker (Figure 1A), as previously described.<sup>15</sup> The particle size was adjusted such that on average only one protein dimer binds to each nanoparticle due to the protein size (Figure S1, Supporting Information).

To demonstrate the passivating properties of the protein repellent polymer, the upper part of the sample was covered only with PEG, whereas the bottom part of the sample was decorated with gold nanoparticles surrounded by PEG (labeled as I and II in Figure 1B,C, respectively). A sharp edge between

the nanopatterned and the non-nanopatterned area was obtained when the coverslips were not completely immersed into the micellar gold solution.

By means of direct and indirect protein-labeling techniques, we determined whether BMP-2 was successfully immobilized on the gold nanoparticle arrays (Figure 1B,C). The coupling of BMP-2 was monitored over a large area of the sample. Figure 1B shows a phosphorimager scan of a coverslip presenting radioactively labeled [<sup>125</sup>I]BMP-2 immobilized on gold nanoparticles with an average interparticle distance of 56 ( $\pm$ 8) nm. The presence of immobilized BMP-2 on the nanopatterned substrates was also confirmed by indirect immunofluorescence staining of the protein and fluorescence microscopy imaging (Figure 1C). Additionally, samples presenting different spacing of gold nanoparticles with immobilized BMP-2 were imaged by chemiluminescence (Figure S2, Supporting Information). All detection methods showed that the protein was selectively immobilized on the gold nanoparticles and did not bind to the protein-repellent side of the sample, thereby confirming the resistance of PEG against unspecific protein adsorption.<sup>20,21</sup>

Atomic force microscopy was used to investigate the height distribution at the surface and thus the presence and distribution of surface-bound biomolecules. AFM measurements were performed to further investigate the gold nanoparticles and to quantitatively visualize BMP-2 molecules on gold nanostructured substrates (Figure 2A–F). To monitor the binding of BMP-2 to gold nanoparticles, a substrate presenting the nanoparticles without BMP-2 and the protein repellent layer was imaged and compared to a substrate where

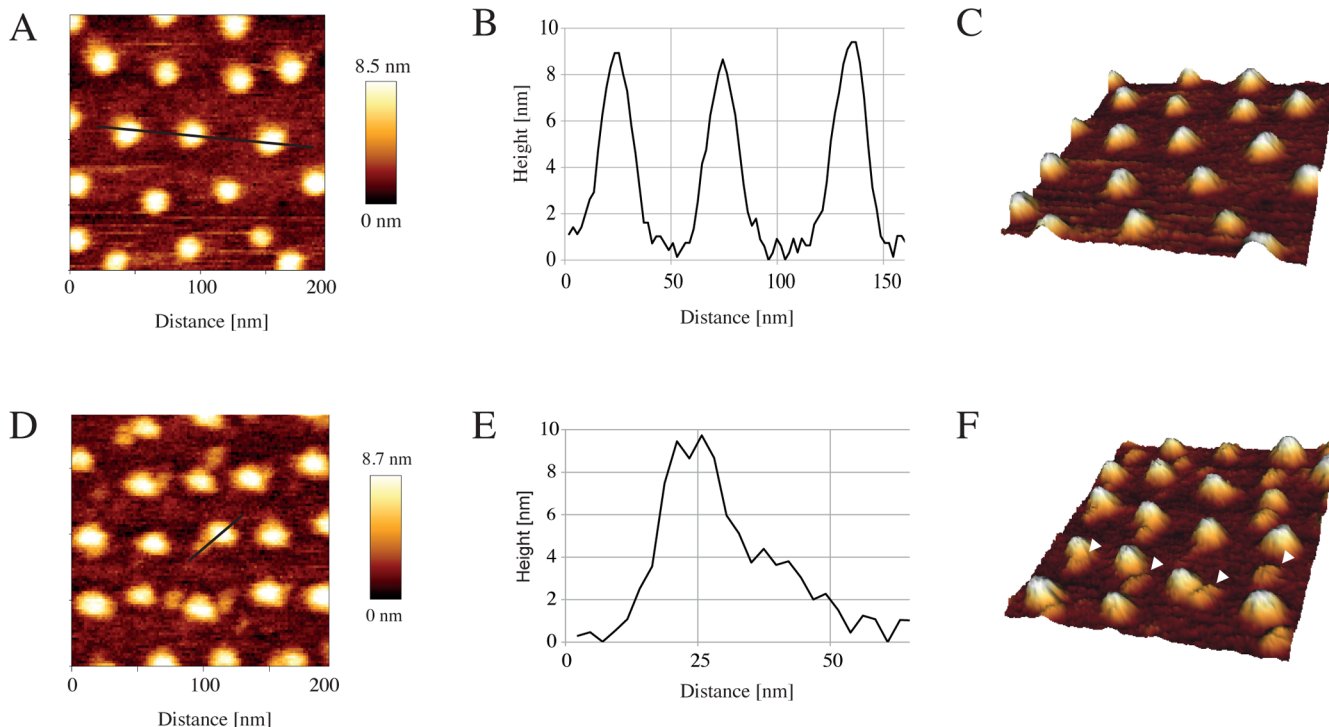


**Figure 2.** Imaging of glass substrates patterned with gold nanoparticles carrying BMP-2; the interparticle surface is covered with PEG. Zoomed-in AFM images of  $200 \text{ nm} \times 200 \text{ nm}$  of passivated surfaces without (A) and with bound BMP-2 (D). The black lines depict the cross sections, which are plotted in panels B and E, respectively. The presence of the “shoulder” of approximately 4 nm in panel E is due to the binding of the protein to the gold nanoparticle. Corresponding 3D-images of panels A and D are shown in panels C and F, respectively, illustrating the presence of the protein in close proximity to a nanoparticle. The arrows indicate BMP dimers.

BMP-2 was bound to the nanoparticles. An area of  $2 \mu\text{m} \times 2 \mu\text{m}$  was scanned in intermittent contact mode in air-dry state. Figure 2A shows a zoom-in image of  $200 \text{ nm} \times 200 \text{ nm}$  of a passivated gold nanostructured substrate without the protein. The black line depicts the cross section that is plotted in Figure 2B. From these measurements, the average particle height was estimated to be approximately 8–9 nm. Figure 2C shows the 3D-image of Figure 2A, confirming the distribution of the particles and their physical properties, such as size, morphology, and surface texture. Figures 2D–F show AFM measurements performed on passivated gold nanostructured substrates with covalently immobilized BMP-2 on the nanoparticles. The height of the gold nanoparticles was similar to the one of the nanoparticles on the nonfunctionalized surface and estimated to be approximately 9 nm, whereas the “shoulder” of approximately 4 nm can be assigned to the iBMP-2 homodimer. The 3D-image of Figure 2D displays iBMP-2 in close proximity to the gold nanoparticles (Figure 2F). The majority of BMP molecules is located at an angle of  $45^\circ$  relative to the gold nanoparticle, which is likely due to the drying of the sample under a nitrogen stream. The quantification of the binding probability is performed by estimating the nanoparticle-BMP-2 binding ratio, indicating that 90% of the gold nanoparticles bind at least one BMP-2 molecule.

Imaging small molecules, such as BMP-2, with an estimated size of approximately  $6.4 \times 3.4 \times 3.0 \text{ nm}$  per dimer (Figure S1, Supporting Information), is a challenging task.<sup>22</sup> Kloss et al. monitored BMP-2 adsorbed on diamond films by single-molecule force spectroscopy and estimated the height of the adsorbed molecules to be approximately 3–4 nm.<sup>23</sup> In agreement with these data, we also detected iBMP-2 dimers bound to gold nanoparticles with an average height of 3–4 nm

in close proximity of the nanoparticles. We further found that approximately 86% of the gold nanoparticles binds one BMP-2 molecule and 4% binds two BMP-2 molecules, whereas only on 10% of the particles there is no bound protein. This might be explained by considering the selectivity and efficiency of the formation of bonds between the linker and the protein. The reaction selectivity of NHS esters to primary amines rather than lysine residues of the protein can be attributed to the  $pK_a$  differences of the groups.<sup>24</sup> Regarding the efficiency of this reaction, it should be noted that several factors, such as primary, secondary, and tertiary structure of BMP-2, protein size, and concentrations, might affect the reaction.<sup>25</sup>

After confirming the suitability of nanostructured surfaces for immobilizing tunable amounts of BMP-2, we next varied the interparticle distance of the gold nanoparticles (as described in the material and methods section) to which BMP-2 was covalently immobilized (Figure 3A). To determine the effects of different surface densities of the immobilized protein on cell responses we chose three different interparticle distances, namely,  $36 \pm 6$ ,  $56 \pm 8$ , and  $118 \pm 18 \text{ nm}$  and quantified the amount of BMP-2 immobilized on the substrates by an enzyme immunoassay. The nanopatterned substrates were imaged by scanning electron microscopy (SEM) to further characterize the order parameter of the particles ( $\Phi$ ) and the interparticle distance ( $d$ ).

Figure 3B shows examples of SEM images of quasi-hexagonal gold nanostructured arrays with interparticle distances of  $36 \pm 6$ ,  $56 \pm 8$ , and  $118 \pm 18 \text{ nm}$ , respectively. The amount of protein immobilized on the surfaces was detected by using a monoclonal antibody against BMP-2, which recognizes only its native conformation. The binding of the antibody was then quantified by measuring the conjugated HRP enzymatic activity

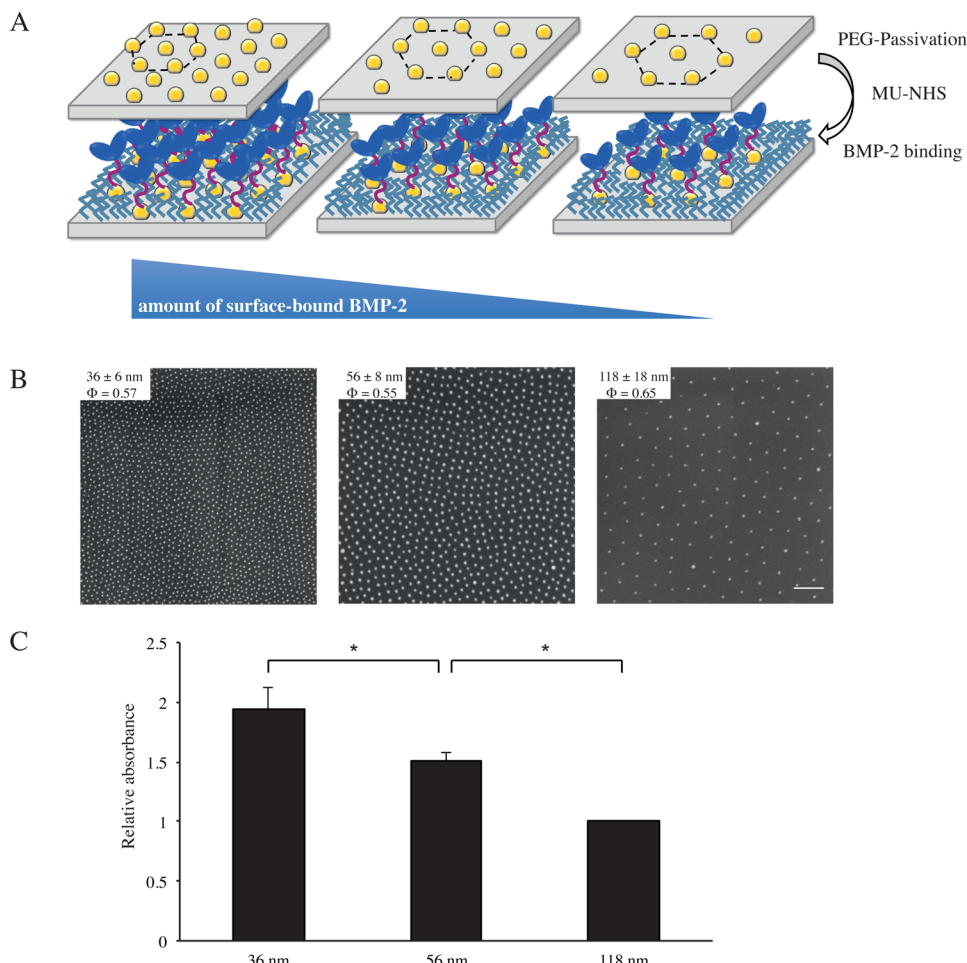


**Figure 3.** Quantification of BMP-2 immobilized on arrays of gold nanoparticles at 36, 56, or 118 nm interparticle spacing. (A) Schematic preparation of BMP-2 immobilization on quasi-hexagonal arrays of gold nanoparticles at different interparticle spacings. With decreasing amount of gold nanoparticles per surface the amount of ibMP-2 per surface decreases (from left to right). (B) SEM images of quasi-hexagonal ordered gold nanoparticle arrays on glass substrates. The inserts indicate the average interparticle distance ( $\pm$ SD) and the order parameter for hexagonal arrangement ( $\Phi$ ); magnification, 50 000 $\times$ ; the scale bar is 200 nm. (C) Enzyme immunoassay measurement of surface immobilized BMP-2. The plot shows the absorbance values at 570 nm of four independent experiments normalized to the value of the largest spacing. Error bars indicate standard deviation (SD),  $p < 0.05$ . Absolute absorption values are summarized in Table S1 (Supporting Information).

using Ampliflu Red as substrate. Figures 3C and S2 (Supporting Information) show that BMP-2 in its native conformation is successfully immobilized on the different types of gold nanopatterns. The absorption values of samples with the highest interparticle distance ( $d = 118 \pm 18$  nm), and therefore with the lowest amount of immobilized protein, were set to 1. Compared to these samples, the amount of immobilized protein was 1.5- and 1.9-fold higher on samples with interparticle distances of  $56 \pm 8$  and  $36 \pm 6$  nm, respectively (Supporting Information Table S1).

The amount of immobilized protein was then estimated by determining the average number of gold nanoparticles per  $\mu\text{m}^2$ . Note that the calculation of the values shown in Table 1 is based on the analysis of SEM images taking into account the order parameter, and not on theoretical values, which would assume a perfectly hexagonal order. The number of gold nanoparticles per  $\mu\text{m}^2$  presenting immobilized BMP-2 was then determined assuming coverage of 90% of the particles with one BMP-2 dimer, as shown in Figure 2 for a substrate having a 56 nm interparticle spacing. Thus, the surface density of the immobilized protein is estimated to be  $3.3 \text{ ng/cm}^2$  (corresponding to an amount of 15 ng per sample) for the 36 nm

**Table 1. Surface Density of Immobilized BMP-2<sup>a</sup>**

interparticle distance [nm]	number of gold nanoparticles per $\mu\text{m}^2$	number of gold nanoparticles with immobilized BMP-2 per $\mu\text{m}^2$	amount of BMP-2 on the surface [ng/cm <sup>2</sup> ]	amount of BMP-2 per sample [ng]
$36 \pm 6$	$846 \pm 62$	$761 \pm 56$	3.3	15
$56 \pm 8$	$299 \pm 21$	$269 \pm 19$	1.1	5
$118 \pm 18$	$48 \pm 11$	$43 \pm 10$	0.2	1

<sup>a</sup>Please note that the calculation of the values is based on SEM image analysis and not on theoretical values assuming a perfectly hexagonal order. The amount of immobilized protein is estimated according to the AFM measurements of nanoparticle coverage with BMP-2.

spacing,  $1.1 \text{ ng/cm}^2$  (5 ng per sample) for the 56 nm spacing, and  $0.2 \text{ ng/cm}^2$  (1 ng per sample) for the 118 nm spacing (see Table 1). In several studies designed to hinder BMP-2 diffusion and subsequent loss, different amounts of the growth factor have been trapped within polymer films, such as PLL/HA or silk fibroin films.<sup>26–28</sup> For example, the sustained effect of BMP-2 has been investigated when loaded into PLL/HA films at a concentration ranging from 750 to 950 ng/cm<sup>2</sup> or, in more recent work, from 50 to 400 ng/mL. These amounts were

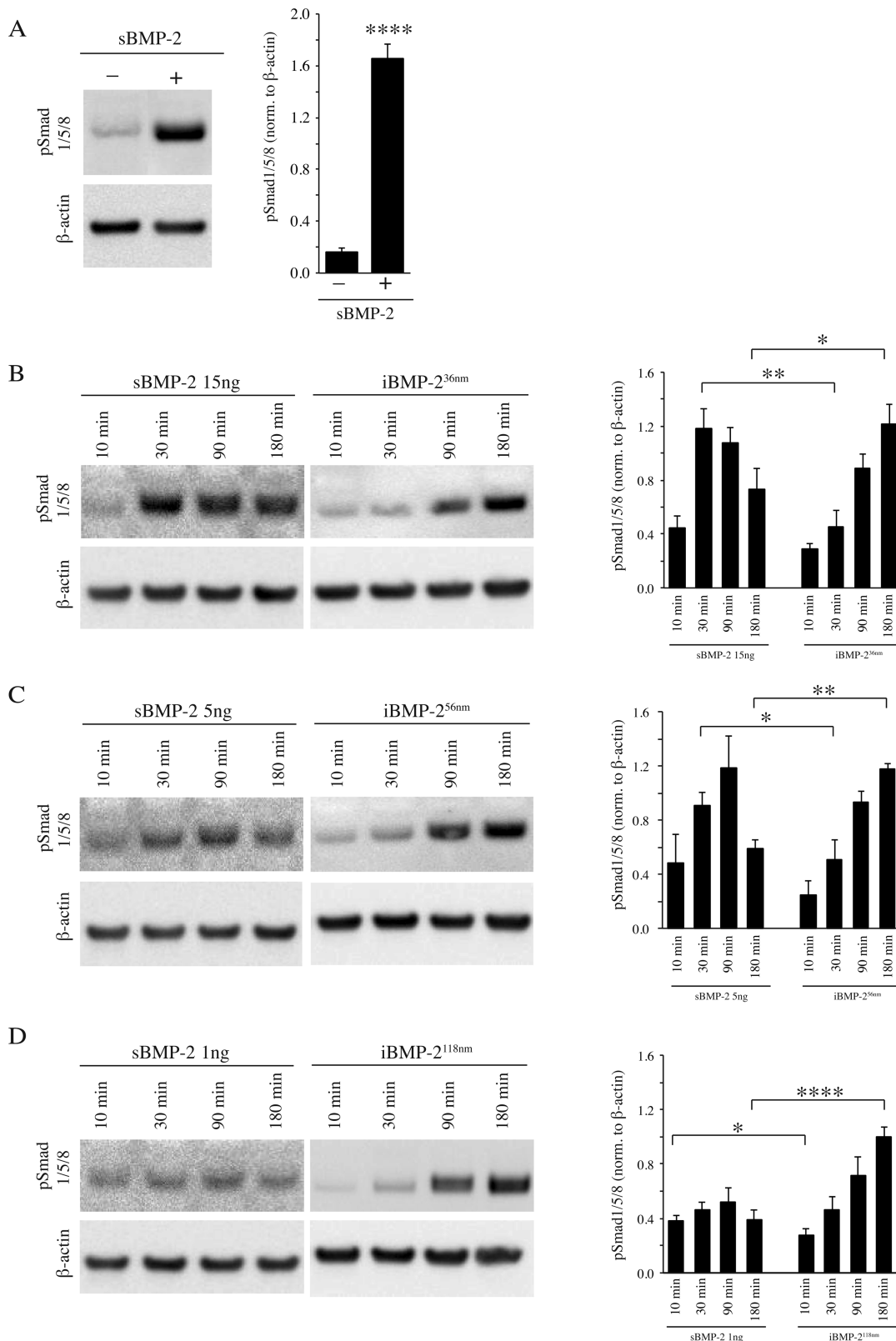


**Figure 4.** Immobilized BMP-2 on gold nanostructures maintains its biological activity and induces Smad signaling. (A) Lysates from C2C12 cells that were not exposed (−) or exposed to 20 nM sBMP-2 (+) for 30 min served as negative or positive control, respectively, and were immunoblotted for pSmad1/5/8 and β-actin. (B–D) Adherent C2C12 cells were stimulated with nanopatterned surfaces with covalently immobilized BMP-2 (iBMP) and surfaces in the presence of the corresponding amount of BMP-2 in cell culture medium (sBMP-2) for 10 min up to 180 min. Phosphorylation levels of Smad1/5/8 were analyzed by Western blot, the intensities of protein bands were quantified and normalized to β-actin levels. Experiments were performed three times, and representative images and plots are shown here. \* $p < 0.05$ , \*\* $p < 0.01$ , \*\*\* $p < 0.0001$ ; the results of the complete statistical significance analysis between all groups are summarized in Table S2 (Supporting Information).

shown to be sufficient to induce osteogenic differentiation in BMP-responsive cells.<sup>26,28</sup> Regarding the covalent immobilization of BMP-2 on materials, it has been reported that the lowest amount that triggers downstream signaling responses is 31 ng/cm<sup>2</sup>; however, this observation has been performed on silk fibroin films in the presence of additional osteogenic stimuli.<sup>27</sup> In comparison to these studies, we present here a method for delivering extremely low albeit precisely tuned amounts of BMP-2. To our knowledge, this is the first study in which growth factors are immobilized on materials at a high spatial resolution to achieve their localized and sustained delivery to cells.

The interaction of BMP-2 with BMP receptor complexes leads to the initiation of intracellular signaling events, depending on the mode of receptor oligomerization.<sup>29</sup> Binding of BMP-2 to so-called preformed complexes (PFCs), consisting of type I and type II receptors,<sup>29–31</sup> initiates canonical Smad signaling by phosphorylation of receptor-regulated Smad proteins 1/5/8 (R-Smads), which then in turn bind to Smad 4 (Co-Smad). This heteromeric complex translocates to the nucleus, thereby regulating transcription of target genes. Additionally, ligand-mediated receptor oligomerization, which is referred to as BMP-induced signaling complex (BISC) formation, triggers other signaling events, such as MAPK activation or activation of the PI3K/Akt pathway,<sup>3,29,32</sup> which is commonly referred to as “non-Smad signaling”.<sup>33</sup>

To determine the signaling events triggered by immobilized BMP-2, we recently coupled BMP-2 to a self-assembled monolayer of the bifunctional linker MU-NHS on gold-coated surfaces. This immobilization strategy proved to be efficient in triggering both short- and long-term canonical Smad and non-Smad signaling responses. Here, it was demonstrated that surface-bound BMP-2 suppresses myogenesis and induces transdifferentiation of C2C12 myoblasts into osteoblasts during a period of 6 days.<sup>15,16</sup>

Although the surface coverage of the protein was estimated to be 70–80 ng/cm<sup>2</sup>, with this approach we could not quantify the threshold amount of immobilized BMP-2 sufficient to trigger signaling responses. In the present work, adherent C2C12 cells were exposed to different amounts of BMP-2 covalently bound to nanostructured surfaces with varying interparticle distances (see Table 1).

Cells cannot firmly adhere and spread on surfaces, which present only nanoparticle arrays and passivated interparticle space, since there are no adhesive molecules on the surface (Figure S3A, Supporting Information). Thus, the nano-patterned substrates we placed on top of a cell monolayer adhering to a culture dish, as described previously<sup>15,16</sup> (Figure S3B, Supporting Information).

The pluripotent mesenchymal precursor cell line C2C12 is able to differentiate and fuse to augment existing muscle fibers and form new fibers.<sup>34,35</sup> However, it has been shown that BMP-2 inhibits the myogenic differentiation of C2C12 cells and further converts their differentiation into osteogenic lineage, inducing elevated levels of ALP activity and osteocalcin production.<sup>36</sup> Since BMP-2 signaling is well characterized in this established cell line we chose these cells as a model system. The phosphorylation state of Smad 1/5/8 proteins, which are direct downstream reporters of the BMP-2 signaling pathway, was used as indicator for the bioactivity of BMP-2.

For comparison, the corresponding amount of BMP-2 was added to the cell culture medium (sBMP-2), and nano-patterned surfaces without the immobilized molecule were

placed on top of the cells. Glass surfaces completely covered with PEG were used as negative control (Figure S3, Supporting Information). The phosphorylation levels of Smad 1/5/8 were determined after 10, 30, 90, or 180 min of stimulation by Western blot analysis of cell protein extracts, and the levels were quantified relative to β-actin (Figure 4). Lysates from cells exposed for 30 min to 20 nM BMP-2 (corresponding to 80 ng of the protein) added to the culture media (sBMP-2) served as positive control,<sup>15</sup> whereas lysates from cells in suspension and not exposed to the growth factor served as negative control (Figures 4A and S4A, Supporting Information).

C2C12 cells exposed to either sBMP-2 (15 to 1 ng) or immobilized BMP-2 (iBMP-2, at 36 to 118 nm interparticle spacing) were analyzed regarding their Smad phosphorylation kinetics (Figure 4B–D). Note that the levels of β-actin in cell lysates mirror the levels of nonphosphorylated Smad1, indicating that Smad phosphorylation is induced by the addition of BMP-2 molecules either in the media or immobilized on the surface (Figure S4B, Supporting Information). Interestingly, while cells in the presence of sBMP-2 show an increase in receptor-mediated C-terminal phosphorylation of Smads already after 30 min, with a decline between 90 and 180 min (Figure 4B,C), the Smad phosphorylation kinetics induced by iBMP-2 is different. For all three conditions, the increase in phosphorylation is observed after 90 min, and it is still present at 180 min after stimulation. Most interestingly, while 1 ng of sBMP-2 is too low to activate the Smad pathway, the corresponding immobilized concentration still leads to a remarkable phosphorylation of Smad 1/5/8, which is sustained even after 180 min of stimulation (Figure 4D). As a non-Smad pathway we have analyzed the phosphorylation of p38-MAPK. We observed an initial trigger of this signaling pathway, which might be due to mechanical stress delivered from the application of the nanostructured surface, thus overlaying the effect of BMP-2 (data not shown).

Although Smad activation is delayed in all cases, the immobilization strategy does not reduce, but rather prolongs and further significantly elevates BMP-dependent short-term signaling compared to stimulation with the soluble growth factor. This becomes particularly evident when comparing Smad phosphorylation in cells stimulated with 1 ng of sBMP-2 or 1 ng of iBMP-2. Hence, in the case of immobilized growth factor, its sustained presentation and not the amount of immobilized BMP-2 affects the phosphorylation kinetics of Smad.

These results were also validated with other BMP-responsive cells. Hence, MC3T3 mouse calvaria osteoblasts were exposed to different amounts of sBMP-2 and iBMP-2, and Smad 1/5/8 phosphorylation was detected. Surface immobilized BMP-2 is inducing Smad phosphorylation in MC3T3 and, in comparison to the same amount of sBMP-2, the phosphorylation levels induced by iBMP-2 are higher (Figure S5, Supporting Information).

**Conclusion.** We have applied BCMN as a nanopatterning tool to immobilize and control growth factor surface density to determine at unprecedented resolution the minimal concentration, which is necessary for triggering signaling responses. Unlike other studies, which investigate the effect of growth factor in combination with adhesion-promoting peptides/proteins or functional molecules<sup>37,38</sup> and which themselves affect cell behavior, this work explored the sole effect of varying amount of immobilized BMP-2 on short-term cellular responses. Our results provide evidence that local application

of BMP-2 in its immobilized form is suitable and most efficient to trigger the Smad-transcriptional pathway, which is essential for osteogenic differentiation of bone precursor cells. In fact, surface-immobilized BMP-2 at a concentration as low as 0.2 ng/cm<sup>2</sup> still induces Smad-dependent signaling, due to its local and sustained presentation without perturbing the growth factor bioactivity.

The delay in the onset of Smad phosphorylation might be explained by the intrinsic lateral mobility of the BMP receptors, which are distinct between BMPRI and BMPRII receptors.<sup>39</sup> Since both receptor subtypes are required for building the signaling receptor complex (PFC) triggering Smad phosphorylation, the lateral mobility of BMPRII might be the rate-limiting step in those conditions, where the ligand is immobilized. Furthermore, our approach suggests that the ligand does not need to be endocytosed to propagate Smad signaling, as indicated by us in previous studies.<sup>15,16</sup> The receptor internalization requires clathrin-mediated endocytosis for BMPRI and both clathrin-dependent and -independent mechanisms for BMPRII.<sup>40</sup> However, the effects of internalization on TGF- $\beta$  and BMP signal transduction are still controversial.<sup>41,42</sup> More recently, Gleason et al. demonstrated that the clathrin-adapter protein AP-2 is essential for BMPRI receptor internalization and signaling in vivo and further suggested that this process does not require ligand binding.<sup>43</sup> In the present study we are not able yet to clarify how receptor trafficking, in the presence of immobilized ligands, might take place at the binding sites. We can speculate that the presentation of immobilized BMP-2 does not affect endocytosis and recycling of the receptors, but might still influence the formation of active heteromeric complexes at the plasma membrane, thus regulating the signaling strength and dynamics of the pathway.

The use of BCMN to pattern growth factor can be further applied to investigate the clustering of BMP receptors and the receptor complex formation in living cells at unprecedented resolution. Our approach might be also a valid tool to quantify the number of receptors, which are bound to the protein and are required for triggering signal transduction. Thus, we can anticipate that such immobilization strategy could become a useful tool for investigating the critical concentration of growth factors and the minimum amount of receptors, which are necessary for activating cell responses.

**Experimental Section. Preparation of Nanopatterned Substrates.** As described in previous work, glass coverslips were decorated with a regular arrangement of gold nanoparticles by using diblock copolymer micellar nanolithography (BCMN).<sup>17,18,21</sup> Briefly, diblock copolymers built up by polystyrene and poly-2-vinylpyridine formed micelles in nonpolar solvents upon a critical concentration. Their polar core could then be loaded with metal precursor salts. Nanostructured surfaces were prepared by dipping the clean substrate into micellar polymer solutions with a defined velocity followed by exposing the formed micellar monolayer to a reactive hydrogen plasma (TePla PS210; 600 W; 0.3 mbar), leaving gold nanoparticles of 5–8 nm diameter on the substrate. These gold nanoparticles were organized in hexagonal patterns and separated by 36 to 118 nm, depending on the size of the copolymer used.<sup>44</sup>

**Passivation and Functionalization of Nanopatterned Substrates.** The space between the gold nanoparticles was then covered with polyethylene glycol (PEG, molecular weight 2000 Da) to prevent cell and protein adhesion.<sup>19</sup> Throughout

the experiments carrier-free recombinant human BMP-2 expressed in *E. coli* (R&D Systems) was used. Gold nanoparticles were decorated with BMP-2 or iodinated BMP-2 by incubating the PEG-functionalized substrates for 4 h at room temperature (RT) with a heterobifunctional linker (1 mM 11-mercaptopoundecanoyl-N-hydroxysuccinimide ester (MU-NHS) in DMF) followed by an incubation with BMP-2 (140 nM in PBS containing 1 M NaCl, pH 8.5) overnight at 4 °C.<sup>15</sup>

**ELISA Based Ampliflu Red Enzyme Assay.** To detect BMP-2 on surfaces, the samples were first incubated with mouse anti-BMP-2 antibody (Sigma) and afterward with goat antimouse horseradish peroxidase (HRP)-conjugated IgG (Santa Cruz Biotechnology). Using the Ampliflu Red assay (Sigma), HRP enzymatic activity was measured at 570 nm with a plate reader (Tecan Infinite M200). Data were plotted as relative absorbance normalized to the control values.

**Scanning Electron Microscopy.** Glass substrates were coated with a layer of graphite (approximately 5 nm) using MED020 Sputter Coater (BAL-TEC AG, Witten) to be imaged with a scanning electron microscope (LEO 1530 or Ultra 55, both Zeiss SMT, Oberkochen) using acceleration voltages of 3 to 15 kV, working distances of 5 to 10 mm, and a pressure of approximately 5 × 10<sup>-6</sup> mbar. The nanoparticle spacing (*d*) was then analyzed using a plug-in for ImageJ (Research Services Branch, Image Analysis Software, NIH, USA). In addition to the interparticle distance *d* also an order parameter ranging from 0 to 1 was defined with 1 representing a perfect order. Only nanopatterned arrays yielding an order parameter above 0.5 were used for experiments.

**Iodination of BMP-2 with Radioactive [<sup>125</sup>I] and Radioluminescence.** Iodination of BMP-2 was performed as described earlier.<sup>15,45</sup> For the detection of [<sup>125</sup>I]BMP-2 on surfaces, samples were imaged with a SLA 5000 phosphor imager (Fuji).

**Fluorescence Microscopy and Indirect Immunofluorescence Staining.** Samples were blocked in 5% (w/v) BSA (Sigma-Aldrich) in PBS (BSA/PBS) solution for 1 h at RT, subsequently incubated with 1:100 anti-BMP-2 mouse IgG (Sigma-Aldrich) for 1 h at RT and finally washed three times in PBS. Samples were incubated with Alexa Fluor 488 goat antimouse IgG (Invitrogen). Before detection, samples were washed three times for 5 min. Immunofluorescence images were acquired on a DeltaVision RT system (Applied Precision Inc.).

**Atomic Force Microscopy.** For detection of the BMP-2 covalently linked to the gold nanoparticles, an atomic force microscope (Nano Wizard, JPK Instruments, Berlin) was used. Samples were prepared as described above and dried in a stream of nitrogen. A sample passivated with PEG 2000 was imaged as a control. The measurements were performed in air-dry state in intermittent-contact mode, using a SCD14 cantilever (nominal spring constant specified by the manufacturer: 5.0 N m<sup>-1</sup>, Schaefer Technologie GmbH, Langen) with a diamond tip. The amplitude was set to 1.5 V, and the Z-range was limited to 5.85 μm. An area of 2 μm × 2 μm was scanned. The data were analyzed with the JPK data processing software.

**Cell Culture.** Mouse C2C12 myoblasts (ATCC CRL-1772) and mouse MC3T3 preosteoblasts (RCB1126), which are known to respond to BMP-2, were used for functional assays. C2C12 cells were cultured as subconfluent monolayers in growth medium, consisting of Dulbecco's modified Eagle's

medium (DMEM) (Gibco BRL) supplemented with 10% heat inactivated fetal bovine serum (FBS) (Sigma) and 1% penicillin/streptomycin (Gibco BRL) at 37 °C and 5% CO<sub>2</sub>. MC3T3 cells were cultured in alpha minimum essential medium containing 2 mM L-glutamine and 1 mM sodium pyruvate (Gibco BRL, #A1049001) supplemented with 10% heat inactivated fetal bovine serum (FBS) (Sigma) and 1% penicillin/streptomycin (Gibco BRL) at 37 °C and 5% CO<sub>2</sub>.

**Protein Isolation and Western Blot Analysis.** To extract total cell proteins 5 × 10<sup>5</sup> cells were seeded in 6-well plates under standard culture conditions. One aliquot containing 5 × 10<sup>5</sup> cells was lysed directly and served as negative control (indicated as cells in suspension). After 24 h the adherent cells were starved in serum-free base medium for 4 h. Cells were stimulated with either 20 nM BMP-2 in base medium or with 15, 5, or 1 ng of growth factor added to 150 μL of base medium (sBMP-2). A glass coverslip was then placed on top of the cell monolayer to maintain the same conditions as for the stimulation with BMP-2 covalently bound to nanostructured surfaces (iBMP-2).

After 30 min the surfaces were gently removed, and the cells inspected by phase contrast microscopy to check for cell integrity. Then, culture medium was removed, and 100 μL of 1× Laemmli buffer (2× Laemmli: 4% (w/v) SDS, 20% (v/v) glycerol, 120 mM Tris-HCl pH 6.8, 31 μg/mL DTT, 0.02% (w/v) bromine phenol blue) was added per well. The culture dish/plate was placed at -80 °C for 1 h, then lysates were transferred into tubes and stored at -20 °C.

Protein extracts were separated by SDS-PAGE, transferred to nitrocellulose membrane and then probed with 1:1000 rabbit anti-p-Smad 1/5/8 (Cell Signaling Technology), 1:1000 rabbit anti-Smad1 ((D59D7) XP, Cell Signaling Technology), and 1:2000 mouse anti-β-actin (Sigma) antibodies. Incubation with 1:5000 goat antirabbit or antimouse HRP-conjugated IgG (Santa Cruz Biotechnology) was followed by detection with ECL Plus Detection Kits (GE Healthcare). ImageJ was used to determine the intensity of pSmad and β-actin bands.

**Statistical Analysis.** Quantification of Western blots was performed using NIH ImageJ. All pair wise comparisons were done by two-tailed Student's *t* test. Comparison of multiple groups was done by one-way analysis of variance (ANOVA). Statistical calculations were performed using GraphPad Prism version 6.0e for Mac OS X (GraphPad Software, La Jolla California USA, [www.graphpad.com](http://www.graphpad.com)), and *p*-values are indicated in given figures with *p*-values of <0.05 considered as statistically significant. All measurements were performed in at least three independent experiments. The means ± SD were calculated.

## ASSOCIATED CONTENT

### Supporting Information

Crystal structures of dimeric BMP-2 (Figure S1), visualization of iBMP-2 on gold nanostructured surfaces via chemiluminescence (Figure S2), absolute absorbance values measured at 570 nm from ELISA based Ampliflu Red enzyme assay (Table S1), nonadherent C2C12 cells on passivated substrates with nanoparticle arrays and scheme of the experimental setup (Figure S3), Western blot analysis of BMP-dependent signaling pathways in mouse C2C12 myoblasts (Figure S4), summary of statistical significance values between the different groups (Table S2), Western blot analysis of BMP-dependent signaling pathways in mouse MC3T3 preosteoblasts (Figure S5). This

material is available free of charge via the Internet at <http://pubs.acs.org>.

## AUTHOR INFORMATION

### Corresponding Author

\*E-mail: ada.cavalcanti-adam@urz.uni-heidelberg.de.

### Notes

The authors declare no competing financial interest.

## ACKNOWLEDGMENTS

E.A.C. is grateful for the support from the Deutsche Forschungsgemeinschaft (DFG SFB TRR79). P.K. acknowledges the support from DFG (SFB 958) and J.S. from DFG (OL239/6-11 SP520/13-1). E.A.C. and J.S. thank the support from the Max Planck Society. E.H.S. is a student member of the international graduate school HBIGS, University of Heidelberg. We also thank Prof. Jennifer Curtis (Georgia Tech, Atlanta, USA) and Dr. Philipp Girard (Institut Jacques Monod Paris, France) for developing the analysis tools to determine the order parameter and the interparticle distance.

## ABBREVIATIONS

AFM, atomic force microscopy; BCMN, block copolymer micellar nanolithography; BMP-2, bone morphogenetic protein-2; BSA, bovine serum albumin; HA, hyaluronic acid; iBMP-2, immobilized bone morphogenetic protein-2; PEG, polyethylene glycol; PLL, poly-L-lysine; MU-NHS, 11-mercaptopoundecanoyl-N-hydroxysuccinimide ester; sBMP-2, soluble bone morphogenetic protein-2; SEM, scanning electron microscopy; TGF-β, transforming growth factor-β

## REFERENCES

- (1) Hogan, B. L. *Curr. Opin. Genet. Dev.* **1996**, *6*, 432–438.
- (2) Horbelt, D.; Denkis, A.; Knaus, P. *Int. J. Biochem. Cell Biol.* **2012**, *44*, 469–474.
- (3) Sieber, C.; Kopf, J.; Hiepen, C.; Knaus, P. *Cytokine Growth Factor Rev.* **2009**, *20*, 343–355.
- (4) Katagiri, T.; Yamaguchi, A.; Komaki, M.; Abe, E.; Takahashi, N.; Ikeda, T.; Rosen, V.; Wozney, J. M.; Fujisawa-Sehara, A.; Suda, T. *J. Cell Biol.* **1994**, *127*, 1755–1766.
- (5) Jeon, O.; Song, S. J.; Kang, S.-W.; Putnam, A. J.; Kim, B.-S. *Biomaterials* **2007**, *28*, 2763–2771.
- (6) Kirker-Head, C. A. *Adv. Drug Delivery Rev.* **2000**, *43*, 65–92.
- (7) van den Dolder, J.; de Ruijter, A. J. E.; Spauwen, P. H. M.; Jansen, J. A. *Biomaterials* **2003**, *24*, 1853–1860.
- (8) Schulz, T. J.; Tseng, Y.-H. *Cytokine Growth Factor Rev.* **2009**, *20*, 523–531.
- (9) Bessa, P. C.; Casal, M.; Reis, R. L. *J. Tissue Eng. Regen. Med.* **2008**, *2*, 81–96.
- (10) Reddi, A. H. *Biochem. Soc. Trans.* **2000**, *28*, 345–349.
- (11) Garamszegi, N.; Garamszegi, S. P.; Shehadeh, L. A.; Scully, S. P. *Mol. Cancer Res.* **2009**, *7*, 319–329.
- (12) Luginbuehl, V.; Meinel, L.; Merkle, H. P.; Gander, B. *Eur. J. Pharm. Biopharm.* **2004**, *58*, 197–208.
- (13) Nakaji-Hirabayashi, T.; Kato, K.; Arima, Y.; Iwata, H. *Biomaterials* **2007**, *28*, 3517–3529.
- (14) Gonçalves, R.; Martins, M. C. L.; Oliveira, M. J.; Almeida-Porada, G.; Barbosa, M. A. *J. Biomed. Mater. Res.* **2010**, *94*, 576–585.
- (15) Pohl, T. L. M.; Boergermann, J. H.; Schwaerzer, G. K.; Knaus, P.; Cavalcanti-Adam, E. A. *Acta Biomater.* **2012**, *8*, 772–780.
- (16) Pohl, T. L. M.; Schwab, E. H.; Cavalcanti-Adam, E. A. *J. Vis. Exp.* **2013**, *78*, e50842.
- (17) Spatz, J. P.; Mössmer, S.; Hartmann, C.; Möller, M.; Herzog, T.; Krieger, M.; Boyen, H.-G.; Ziemann, P.; Kabius, B. *Langmuir* **2000**, *16*, 407–415.

- (18) Glass, R.; Mller, M.; Spatz, J. P. *Nanotechnology* **2003**, *14*, 1153–1160.
- (19) Blümmel, J.; Perschmann, N.; Aydin, D.; Drinjakovic, J.; Surrey, T.; López-García, M.; Kessler, H.; Spatz, J. P. *Biomaterials* **2007**, *28*, 4739–4747.
- (20) Hirschfeld-Warneken, V. C.; Arnold, M.; Cavalcanti-Adam, A.; López-García, M.; Kessler, H.; Spatz, J. P. *Eur. J. Cell Biol.* **2008**, *87*, 743–750.
- (21) Arnold, M.; Cavalcanti-Adam, E. A.; Glass, R.; Blümmel, J.; Eck, W.; Kantlehner, M.; Kessler, H.; Spatz, J. P. *ChemPhysChem* **2004**, *5*, 383–388.
- (22) Scheufler, C.; Sebald, W.; Hülsmeyer, M. *J. Mol. Biol.* **1999**, *287*, 103–115.
- (23) Kloss, F. R.; Gassner, R.; Preiner, J.; Ebner, A.; Larsson, K.; Hächl, O.; Tuli, T.; Rasse, M.; Moser, D.; Laimer, K.; Nickel, E. A.; Laschober, G.; Brunauer, R.; Klma, G.; Hinterdorfer, P.; Steinmüller-Nethl, D.; Lepperdinger, G. *Biomaterials* **2008**, *29*, 2433–2442.
- (24) Sélo, I.; Négroni, L.; Crémignon, C.; Grassi, J.; Wal, J. M. *J. Immunol. Methods* **1996**, *199*, 127–138.
- (25) Hermanson, G. T. *Bioconjugate Techniques*, 3rd ed.; Academic Press: New York, 2013; p 1200.
- (26) Crouzier, T.; Fourel, L.; Boudou, T.; Albigès-Rizo, C.; Picart, C. *Adv. Mater.* **2011**, *23*, H111–8.
- (27) Karageorgiou, V.; Meinel, L.; Hofmann, S.; Malhotra, A.; Volloch, V.; Kaplan, D. *J. Biomed. Mater. Res.* **2004**, *71*, 528–537.
- (28) Almodóvar, J.; Guillot, R.; Monge, C.; Vollaire, J.; Selimović, Š.; Coll, J.-L.; Khademhosseini, A.; Picart, C. *Biomaterials* **2014**, *35*, 3975–3985.
- (29) Nohe, A. *J. Biol. Chem.* **2001**, *277*, 5330–5338.
- (30) Dijke ten, P.; Yamashita, H.; Sampath, T. K.; Reddi, A. H.; Estevez, M.; Riddle, D. L.; Ichijo, H.; Heldin, C. H.; Miyazono, K. *J. Biol. Chem.* **1994**, *269*, 16985–16988.
- (31) Koenig, B.; Cook, J.; Wolsing, D. H.; Ting, J.; Tiesman, J. P.; Correa, P. E.; Olson, C. A.; Pecquet, A. L.; Ventura, F.; Grant, R. A.; Chen, G.-X.; Wrana, J. L.; Massagué, J.; Rosenbaum, J. S. *Mol. Cell. Biol.* **1994**, *14*, 5961–5974.
- (32) Xiao, Y.-T.; Xiang, L.-X.; Shao, J.-Z. *Biochem. Biophys. Res. Commun.* **2007**, *362*, 550–553.
- (33) Hiemenz, C.; Benn, A.; Denkis, A.; Lukonin, I.; Weise, C.; Boergermann, J. H.; Knaus, P. *BMC Biol.* **2014**, *12*, 43.
- (34) Yaffe, D.; Saxel, O. *Nature* **1977**, *270*, 725–727.
- (35) Blau, H. M.; Webster, C.; Chiu, C. P.; Guttman, S.; Chandler, F. *Exp. Cell Res.* **1983**, *144*, 495–503.
- (36) Katagiri, T.; Akiyama, S.; Namiki, M.; Komaki, M.; Yamaguchi, A.; Rosen, V.; Wozney, J. M.; Fujisawa-Sehara, A.; Suda, T. *Exp. Cell Res.* **1997**, *230*, 342–351.
- (37) Moore, N. M.; Lin, N. J.; Gallant, N. D.; Becker, M. L. *Acta Biomater.* **2011**, *7*, 2091–2100.
- (38) Kim, S. E.; Song, S.-H.; Yun, Y. P.; Choi, B.-J.; Kwon, I. K.; Bae, M. S.; Moon, H.-J.; Kwon, Y.-D. *Biomaterials* **2011**, *32*, 366–373.
- (39) Guzman, A.; Zelman-Femiak, M.; Boergermann, J. H.; Paschkowsky, S.; Kreuzaler, P. A.; Fratzl, P.; Harms, G. S.; Knaus, P. *J. Biol. Chem.* **2012**, *287*, 39492–39504.
- (40) Hartung, A.; Bitton-Worms, K.; Rechtman, M. M.; Wenzel, V.; Boergermann, J. H.; Hassel, S.; Henis, Y. I.; Knaus, P. *Mol. Cell. Biol.* **2006**, *26*, 7791–7805.
- (41) Di Guglielmo, G. M.; Le Roy, C.; Goodfellow, A. F.; Wrana, J. L. *Nat. Cell Biol.* **2003**, *5*, 410–421.
- (42) Chen, C.-L.; Hou, W.-H.; Liu, I.-H.; Hsiao, G.; Huang, S. S.; Huang, J. S. *J. Cell. Sci.* **2009**, *122*, 1863–1871.
- (43) Gleason, R. J.; Akintobi, A. M.; Grant, B. D.; Padgett, R. W. *Proc. Natl. Acad. Sci. U.S.A.* **2014**, *111*, 2578–2583.
- (44) Lohmüller, T.; Aydin, D.; Schwieder, M.; Morhard, C.; Louban, I.; Pacholski, C.; Spatz, J. P. *Biointerphases* **2011**, *6*, MR1–12.
- (45) Frolik, C. A.; Wakefield, L. M.; Smith, D. M.; Sporn, M. B. *J. Biol. Chem.* **1984**, *259*, 10995–11000.